Electronic Supplementary Material (ESI) for Nanoscale.

Supporting information

Chemisorption of nitronyl-nitroxide radicals on gold surface: an assessment of morphology, exchange interaction and decoherence time.

Lorenzo Poggini,[a,b*] Alessandro Lunghi,[a,§] Alberto Collauto,[c,₸] Antonio Barbon,[c] Lidia Armelao,[c,d,e] Agnese Magnani,[f] Andrea Caneschi,[g] Federico Totti,[a*] Lorenzo Sorace,[a,*] Matteo Mannini[a]

[a] Department of Chemistry ''Ugo Schiff'' and INSTM Research Unit, University of Florence, I-50019 Sesto Fiorentino, Italy. E-mail: lorenzo.sorace@unifi.it, federico.totti@unifi.it
[b] ICCOM-CNR, via Madonna del Piano 10, 50019 Sesto, Fiorentino, Italy E-mail: lpoggini@iccom.cnr.it
[c] Department of Chemical Sciences and INSTM Research Unit, University of Padua, I-35131 Padova, Italy
[d] Institute of Condensed Matter Chemistry and Technologies for Energy, National Research Council of Italy, ICMATE-CNR, via Marzolo 1, 35131 Padua, Italy
[e] Department of Chemical Sciences and Materials Technologies, National Research Council of Italy, DSCTM - CNR, Piazzale A. Moro 7, 00185 Rome, Italy
[f] Department of Biotechnologies, Chemistry and Pharmacy, and INSTM Research Unit, University of Siena I-53100 Siena, Italy
[g] DIEF – Department of Industrial Engineering and INSTM Research Unit, University of Florence, Via S. Marta 3, I-50139 Florence, Italy
[₸] present address Centre for Pulse EPR Spectroscopy, Department of Chemistry, Imperial College London, UK
[§] present address: School of Physics, CRANN Institute, AMBER centre, Trinity College, Dublin 2, Ireland

Experimental section

Monolayer preparation

Monolayers of 1 were prepared by immersing flame-annealed Au(111)/mica substrates in a 2 mM dichloromethane solution of the complex for 20 h. The gold slabs were then washed several times under nitrogen atmosphere in the same pure solvent. A bulk reference sample was prepared as thick film by drop casting 50 μL of a 2 mM dichloromethane solution of the complexes on similar gold substrates. All sample preparations were carried out under dry nitrogen atmosphere in a portable glove-bag.

ToF-SIMS

ToF-SIMS analysis was carried out with a TRIFT III time-of flight secondary ion mass spectrometer (Physical Electronics, Chanhassen, MN, USA) equipped with a gold liquid-metal primary ion source (see SI for details). Positive spectra were acquired with a pulsed primary ion beam, by rastering the ion beam over a 100 μm × 100 μm sample area. Positive ion spectra were acquired with a pulsed, bunched 22 keV Au_3^+ primary ion beam, by rastering the ion beam over a 100 μm x 100 μm sample area. The primary ion dose was kept below 10^{11} ions/cm^2 to maintain static SIMS conditions. Positive mass spectra were calibrated to CH_3^+ (m/z 15.023), $C_2H_3^+$ (m/z 27.023), $C_3H_5^+$ (m/z 41.039). The mass resolution (m/Δm) was up to 6000 measuring bulk 1, 5000 on the monolayer of 1. These variations do not alter significantly our analysis. Theoretical isotopic patterns for the most relevant signals were calculated with Molecular Weight Calculator.[1]

XPS

XPS measurements XPS measurements were performed on a Perkin-Elmer PHI 5600-ci spectrometer using a monochromatised (1486.6 eV) Al K_α radiation (15 kV, 300 W). The sample analysis area was 800 mm in diameter, and the working pressure in the order of 10^{-9} mbar. The spectrometer was calibrated assuming the binding energy (BE) of the Au*4f*$_{7/2}$ line at 83.9 eV. Samples were mounted on steel holders under dry nitrogen environment in a portable glove bag which was then connected to the fast-entry lock system of the XPS analytical chamber, in order to minimise air exposure and atmospheric contamination. Detailed scans were

recorded for the N*1s*, S*2p* and Au4f XPS peaks. XPS spectra were recorded in normal emission with the X-ray source mounted at an angle of 54.44° with respect to the analyser and using a pass energy of 40 eV. The analysis involved a liner background subtraction and the single-peak components were deconvoluted by a mixed Gaussian and Lorentzian function (30/70). Spectra were analysed using the CasaXPS software. The atomic composition of the samples was calculated by peak integration, using sensitivity factors provided by the spectrometer manufacturer (PHI V5.4A software) and taking into account the geometric configuration of the apparatus. The experimental uncertainty on the reported atomic composition values does not exceed 5%.

STM

STM measurements were performed with a P47-Pro system (NT-MDT, Zelenograd, Moscow, Russia) equipped with a customized low-current STM head and Pt/Ir 90/10 mechanically-etched tips prepared immediately before use. The bias voltage was applied to the sample. All STM measurements were carried out at room temperature, under N_2 atmosphere.

EPR

An ELEXSYS Bruker EPR spectrometer was used to run all EPR experiments. The spectrometer was equipped with a dielectric cavity inserted in a CF935 Oxford cryostat cooled with vapours of liquid helium.

For Pulse EPR experiments, the cavity was overcoupled in order to have a better bandwidth with a time resolution of few ns. 16 ns π/2 pulses were used for both the EDEPR spectra and the Hahn decay profiles. In order to better extract the decay time of the slow relaxing species (isolated radicals), an off-resonance Hahn echo decay was subtracted (see the on-resonance and off-resonance positions in Fig. 3a). The major contribution of the off-resonance was mainly in the imaginary part, meaning that, mostly, it was due to either signals from high-spin states (i.e. metals in the substrate), or from the cavity.

Computational details

The Au(111) surface has been modelled as a three-layer orthorhombic slab of gold. Each layer consists of 36 gold atoms. The dimensions of the AIMD simulation cell are 17.31 x 14.99 x 60.00 Å. The periodic boundary conditions are always applied in all directions and the size of the box has been chosen to arrange four Nits so that they can form a (3 x 3) unit cell as suggested by the STM image reported for their SAM in [2] The z dimension is long enough to avoid interactions between periodic images of the slabs. Indeed, they are at least 45 Å apart from each other. Experimental and computational evidences[3,4] determined that both thioacetyl and simple thiols once adsorbed on Au(111) undergo a homolytic cleavage of the S–Ac (S–H) leading to the formation of a sulphur radical (-S·) species. For such a reason, we considered only the latter species as bound to the metallic substrate.[5–7] Clean (**Au_{clean}**) and reconstructed (**Au_{recon}**) model surfaces were used. In the latter, the four sulphur radicals interact with four added adatoms in fcc positions. Same fcc positions were chosen to adsorb the sulphur radicals on **Au_{clean}**. AIMD calculations within the Born–Oppenheimer framework have been performed by optimizing the wave function at each MD step. The electronic structure and nuclear forces have been calculated at the meta-GGA DFT level of theory (TPSS) [8] together with Grimme's D3 corrections [9] to account for the dispersion forces within the Gaussian and plane wave (GPW) method, [10] as implemented in CP2K.[11] The GPW approach is based on the expansion of the valence electron molecular orbitals in Gaussian type orbital basis sets, for which we use molecule optimized basis sets of the DZVP-MOLOPT-SR-GTH type.[12] The auxiliary plane wave basis set is needed for the representation of the electronic density in the reciprocal space and the efficient solution of Poisson's equation. We truncate the plane wave basis set at 500 Ry. The Hamiltonian equations of motion are numerically integrated using the velocity Verlet algorithm and a time step of 1 fs (doubling the mass of the hydrogen atoms it was possible to reduce the energy drift less than 0.2 $kcalmol^{-1}$ ps^{-1}). The canonical distribution of momenta at 300 K is enforced using a canonical stochastic rescaled velocity (CSVR) thermostat [13] at a time constant of 50 fs during thermalization and 3000 fs during acquisition runs. A second equivalent AIMD run was performed to explore the new conformational minima. The total energy

conservation has been obtained by smearing the occupation numbers of molecular orbitals with a Fermi–Dirac distribution at 500 K and with a convergence threshold criterion on the maximum wave function gradient of 5.0 x 10^{-5}. The thermalization of the clean and reconstructed cells was performed starting from optimized geometries with consequent temperature increase until the value of 300 K is reached within 4 ps. Initial geometries were obtained by optimization runs were wave function gradient of 1.0 x 10^{-6}. The threshold for the atomic forces during the geometry optimization runs was set to 0.003 Hartree a_0^{-1}, where a_0 is the Bohr radius. Same optimization protocol has been applied to statistically relevant geometries. Energetics in tables are reported per single Nit. The STM images were simulated within the Tersoff−Hamman approximation.[14] The study on how the spin density changes on different scenarios, four geometries were considered (only one Nit each): $\mathbf{1_{iso}}$, $\mathbf{1@Au_{up}}$, and two related to $\mathbf{1@Au_{clean,up}}$ where the single Nit is oriented in a parallel and orthogonal fashion to the gold surface: $\mathbf{1@Au_{clean,down,\parallel}}$ and $\mathbf{1@Au_{clean,down,\perp}}$, respectively. These two geometries were optimized starting from guess geometries obtained as AIMD snapshots. A bridge position was found for all three cases. $\mathbf{Au_{recon}}$ surface was not considered since the $\mathbf{1@Au_{recon,up}}$ converged to very similar geometries after AIMD runs.

Calculation of magnetic interactions

The isotropic exchange couplings have been computed on the optimized snapshot structures (*vide supra*) using the broken symmetry (BS) approach[15,16] through the calculation of the HS spin (↑↑↑↑) state and three $m_s = 0$ BS multiplets: BS1 (↓↓↑↑), BS2 (↓↑↓↑), and BS3 (↑↓↓↑). On the base of the optimized geometries, the spin Hamiltonian has the form: $H = J_1(S_1S_3 + S_2S_4) + J_2(S_1S_4) + J_3(S_1S_2 + S_3S_4) + J_4(S_1S_4)$ where ferromagnetic couplings have negative J values while positive for the antiferromagnetic ones. The scheme is reported here below.

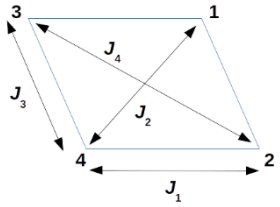

Scheme 1 Exchange coupling scheme where **1**,**2**,**3**,**4** are the Nit centers and J_x (x=1-4) are the four exchange coupling constants defined in the spin Hamiltonian (*vide supra*).

The two geometries **1@Au$_{clean,up}$** and **1@Au$_{clean,down}$** have been used to verify if and how much the gold surface could be involved in the coupling of the Nits' unpaired electrons, a super-exchange bus. **1@Au$_{recon,up}$** and **1@Au$_{recon,down}$** were not considered for their similarities with the respective clean scenarios. Following the protocol used in [17] , the B3LYP [18,19] functional was used for the optimized structures where the gold surface is solidly removed, **-@Au**; revPBE [20] functional was used for both **@Au** and **-@Au**. A convergence threshold criterion on the maximum wave function gradient of 1.0 x 10^{-8}**.** The computed spin densities have been used to verify the correctness of the BS solutions.

Simulation of the STM images

STM images were simulated (see Figure S12) for the four possible scenarios. The two upstanding conformations (**1@Au$_{clean,up}$** and **1@Au$_{recon,up}$**) show similar features: four spots with a butterfly shape with a ribbon-like background. The former should be the fingerprint of the NOs π* orbitals while the latter can be assigned to the sulphur p-orbitals parallel to the surface. These features are more defined for the **1@Au$_{recon,up}$**. On the contrary, the two lying down conformations show completely different features. In **1@Au$_{clean,down}$** the Nit group can be identified by the yellow bright large spots while the darkest ones can be attributed to the rest of the molecule. In **1@Au$_{recon,down}$** the fine details of the whole structure are more evident and along the bright yellow spots it is possible to identify the aromatic rings

shapes next to them (light orange in Figure). The four images have been compared to experimental STM reported in [2] which was collected at room temperature and under nitrogen atmosphere. Despite the non-optimization of the deposition procedure at that time, such images represent the best reference to which we can compare our computational results. In all four scenarios a hexagonal unit cell A x B was computed, with parameters which agree with the experimental ones within the uncertainties.

	N1s	**S2p**
Experimental SAM	61.2%	38.8%
Theoretical	66.7%	33.3%

Table S1. Comparison of theoretical and XPS semiquantitative analysis on N*1s* and S*2p* for the SAM sample.

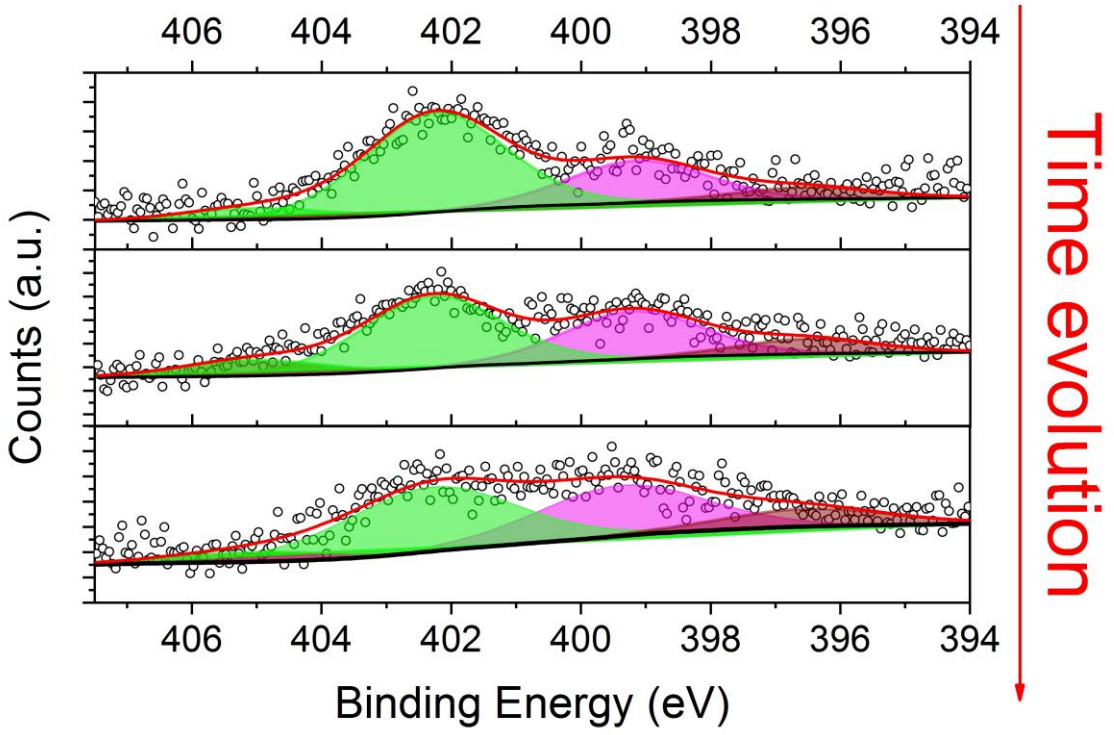

Figure S1. Time evolution of Nitrogen 1s XPS spectrum due to radiation damage under X-Ray in bulk sample.

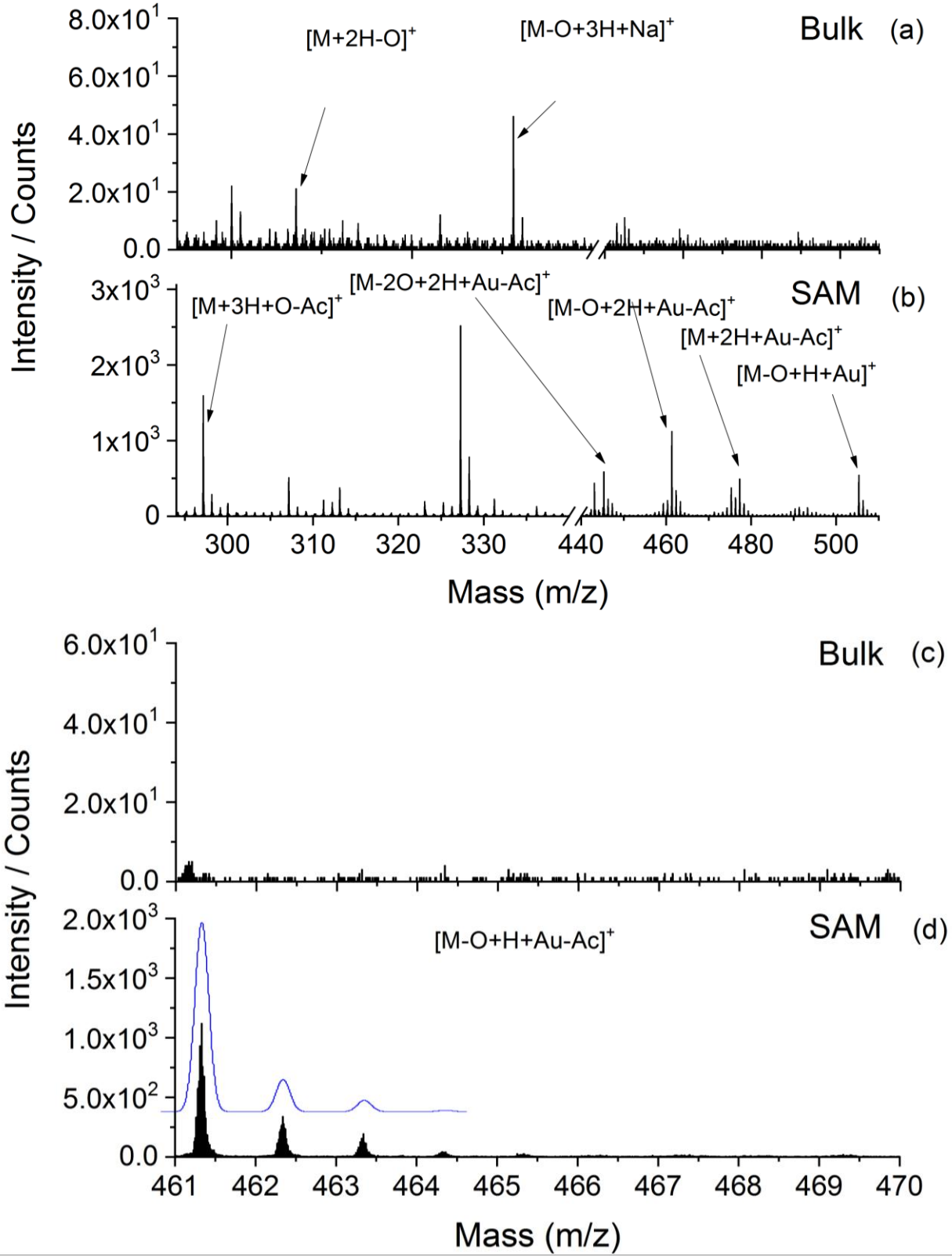

Figure S2. Positive ion ToF-SIMS spectra of (a,c) bulk (**1**) ; (b,d) monolayer of (**1**) prepared from 3mM solution. In (c) and (d) an high resolution scan of the region from 461 to 470 m/z is reported indicating the simulated isotopic distribution pattern of the NNR system chemisorbed to gold.

Table S2 Assignment of positive ion ToF-SIMS spectra of **1** in bulk phase and as SAM

Ion assignment	Teor (m/z)	Bulk	SAM
$[M - O + H + Au]^+$	505.1	-	505.3(vw)
$[M - O - Ac + 2H + Au]^+$	461.1	-	461.3 (m)
$[M - 2O - Ac + 4H + Au]^+$	447.1	-	447.3(w)
$[M - 2O - Ac + 2H + Au]^+$	445.1	-	445.3 (vw)
$[M - O + 3H + Na]^+$	331.1	331.2 (vw)	-
$[M + 2H]^+$	323.1	323.1 (vw)	323.1 (vw)
$[M - 3H - Ac + 2O]^+$	313.1	-	313.1 (vw)
$[M - O + 2H]^+$	307.1	307.2 (vw)	307.2 (vw)
$[M+3H- Ac +O]^+$	297.1	-	297.2 (m)
$[M - 2O + 2H]^+$	291.2	291.2 (w)	291.2 (vw)
$[M - Ac + 2H]^+$	281.1	-	281.1 (w)
$[M - 2O - Ac + 2H]^+$	247.1	-	247.2 (m)

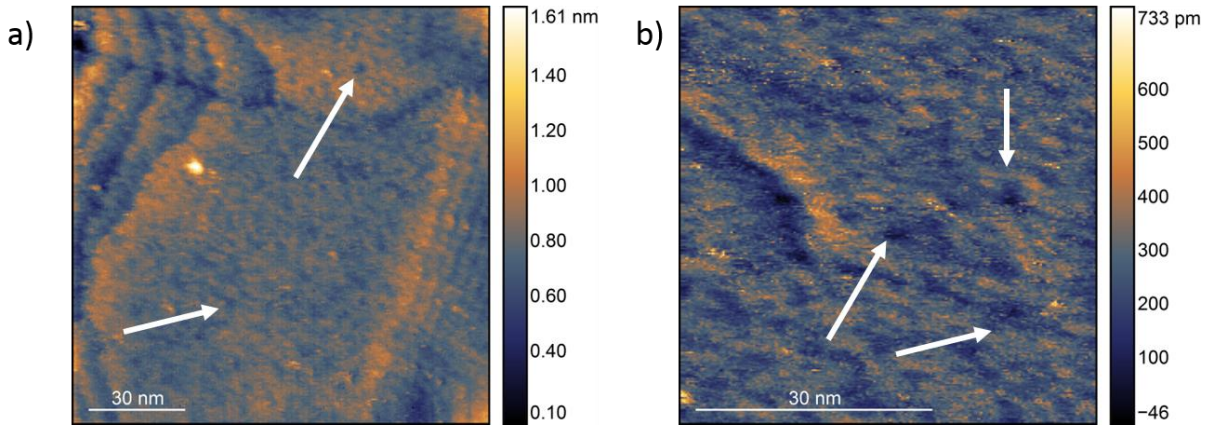

Figure S3. STM images, at two different scales, acquired at room temperature on SAM of **1** on gold obtained from a 3mM solution incubated at 60°C for 24h (V_b=630mV, I_t=120pA). The arrows indicate the presence of pinholes.

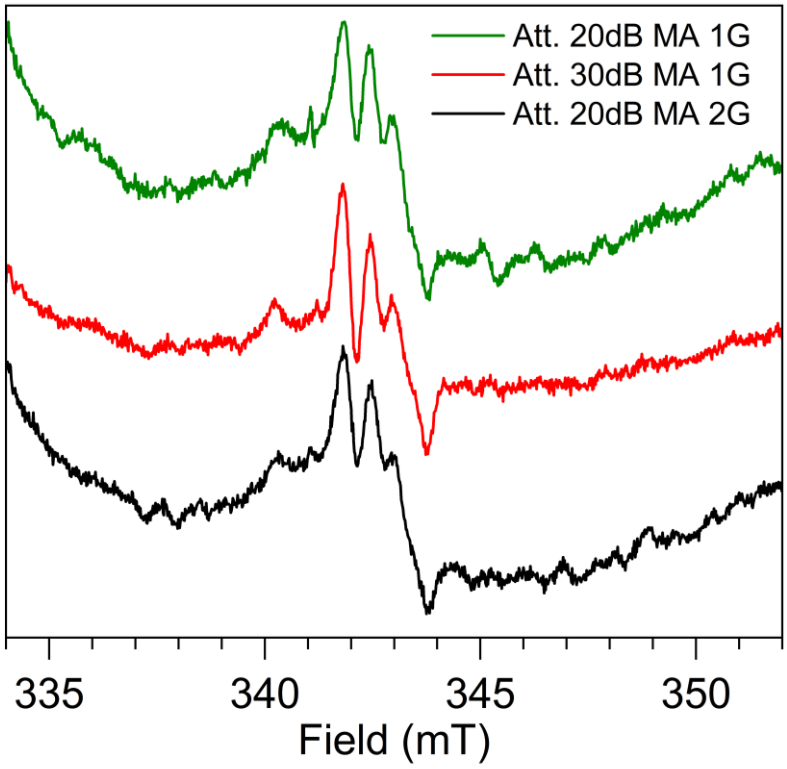

Figure S4 Power dependence of the cw-EPR spectrum of a SAM of **1** at room temperature: Measurement frequency: ν = 9.642 GHz

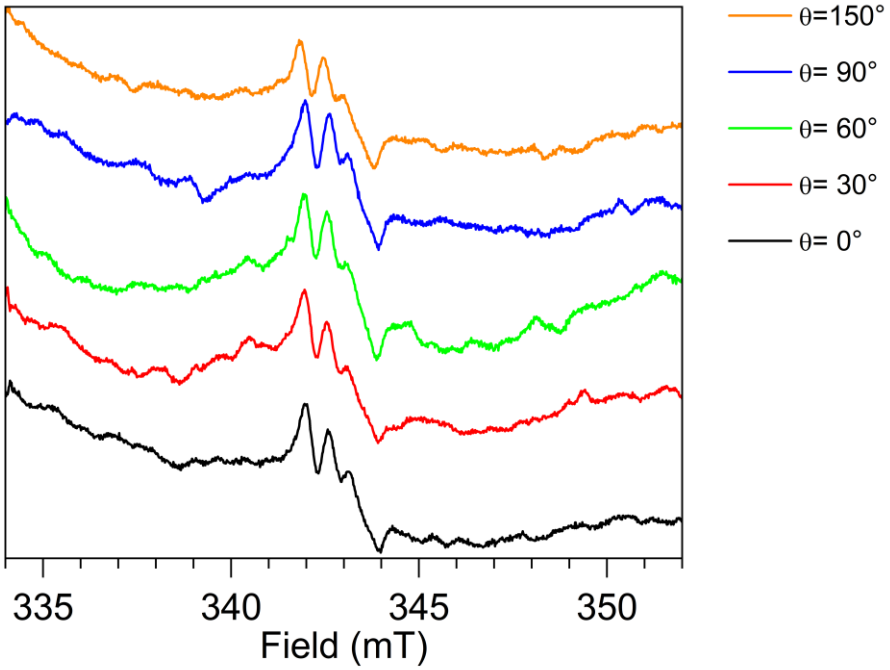

Figure S5 cw-EPR spectrum of a SAM of **1** at room temperature as a function of the angle between the static field and the gold substrate surface. Attenuation: 20 dB; measurement frequency: ν = 9.642 GHz, Modulation amplitude: 0.1 mT

	X-component	Y-component	Z-component
g	2.0111	2.0067	2.0021
A_{N1}/mT	0.08	0.08	1.86
A_{N2}/mT	0.08	0.08	1.86
D/MHz	510 (pair)		

Table S3 parameters used for the simulation of the spectrum in Fig. 2 as superposition of isolated radicals (70 %) and spin-interacting pairs or radicals (30%).

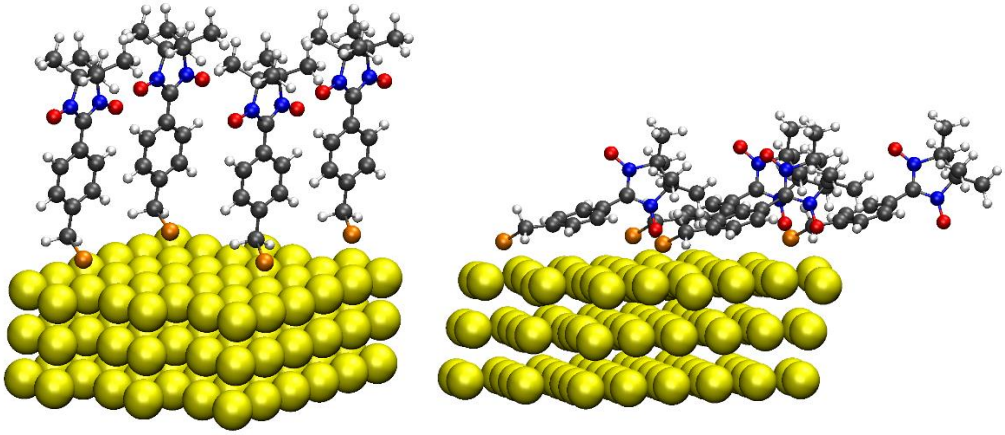

Figure S6. Evolution of the radical configuration on Au clean surface according to AIMD calculations: from a stand-up position to a laid down one, which is maintained to the end of the thermalization stage and for all the following simulation time.

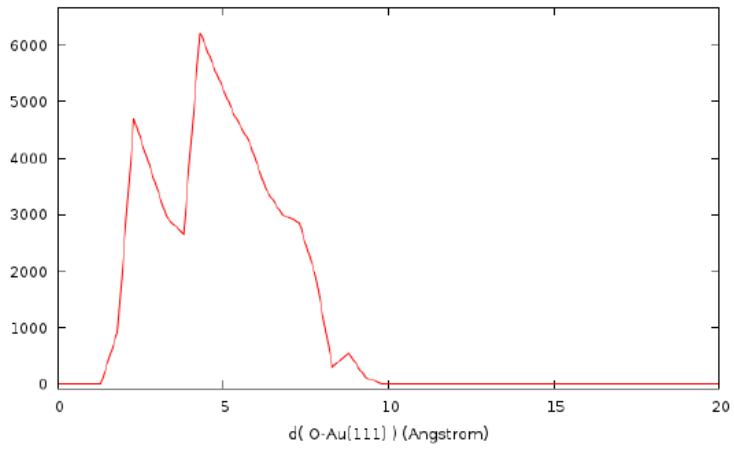

Figure S7. Distribution of the distances between the oxygen atoms and the Au(111) surface for **1Au$_{clean,down}$**

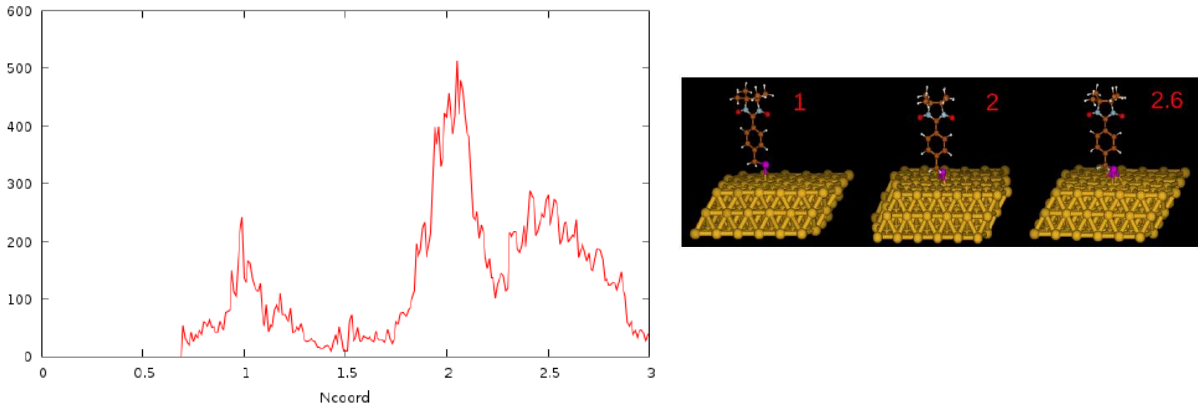

FigureS8. a) Distribution of the coordination number, N_{coord}, of the Sulphur atom with respect the Gold atoms. N_{coord}, has been computed through the relation $\sum_i^{Ns}\sum_j^{NAu}\frac{1-(r_{ij}/R_C)^p}{1-(r_{ij}/R_C)^q}$, where p, q, and R_C where chosen as 8, 18, and 3.18, respectively. b) Reference values for the coordination number for the most relevant geometries.

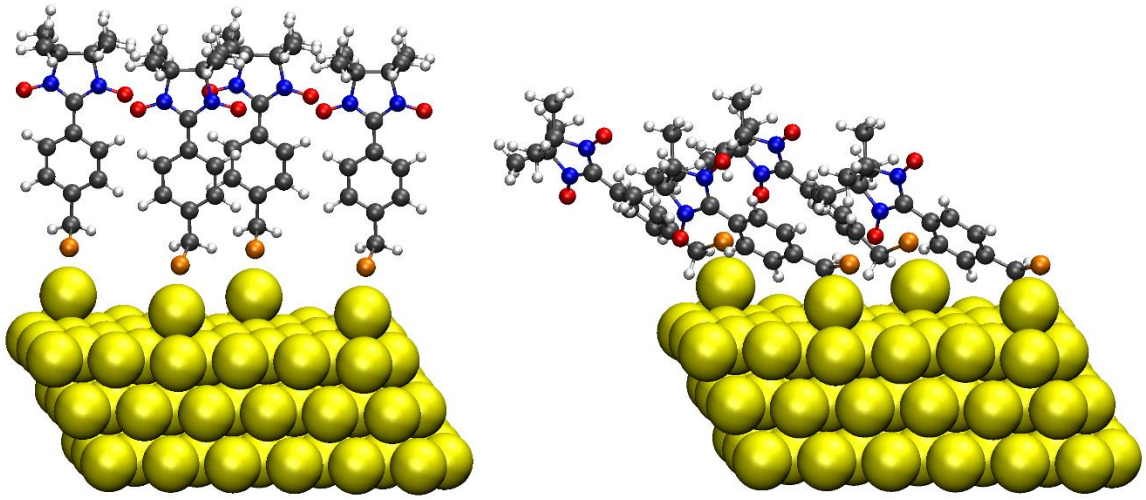

Figure S9 Evolution of the radical configuration on Au reconstructed surface according to AIMD calculations: from a stand-up position to a laid down one, which is maintained to the end of the thermalization stage and for all the following simulation time.

	A	B	C
Nit@Au$_{clean,up}$	8.8	7.8	3.5
Nit@Au$_{clean,down}$	9.0	8.0	3.0
Nit@Au$_{recon,up}$	8.9	7.5	3.0
Nit@Au$_{recon,down}$	8.5	7.7	3.8-5.8
Experiment	9.6	8.1	3.3-5.3

Table S4 Geometrical parameters of the unit cell individuated by the adsorbed Nit radicals (A and B) and the distance between the two NOs within a single Nit (C). Distances are in Å.[2]

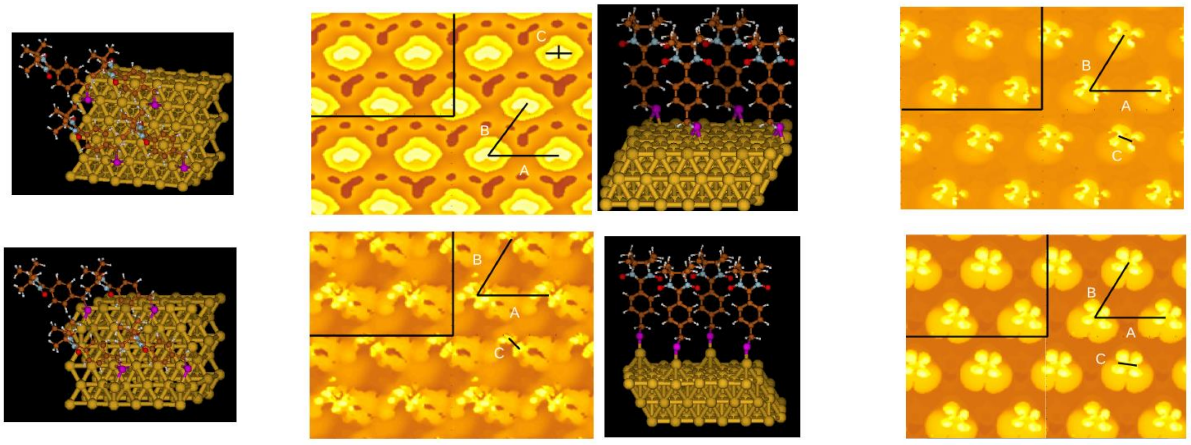

Figure S10 upper panels: simulated STM images and corresponding radical configuration (right: laid down; left: standing up) for **Au$_{clean}$** surface; lower panels: simulated STM images and corresponding radical configuration (right: laid down; left: standing up) for **Au$_{recon}$** surface

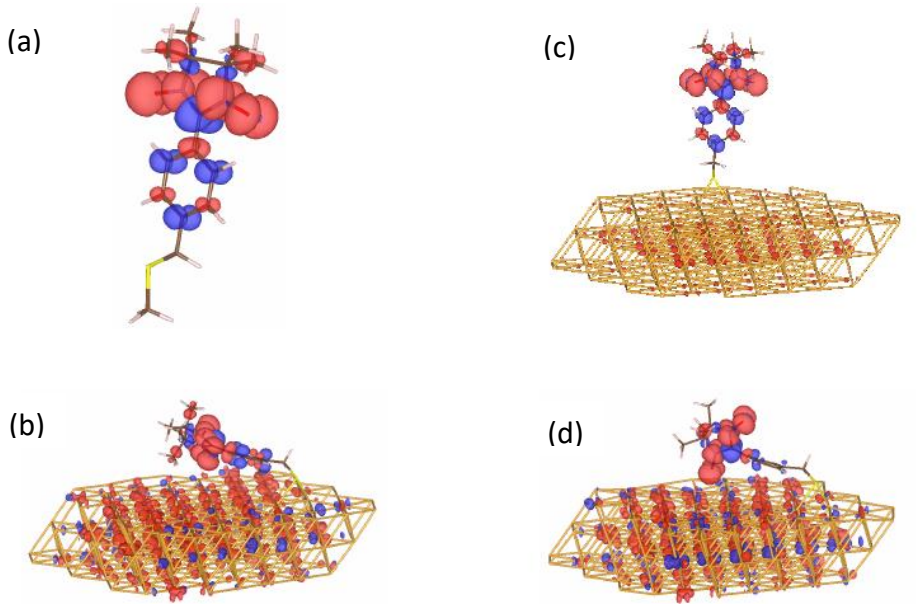

Figure S11 Graphical representation of the calculated spin density for the four cases reported in Table 3, main text.

References

1 Molecular Weight Calculator, http://omics.pnl.gov/software/MWCalculator.php.

2 G. Rajaraman, A. Caneschi, D. Gatteschi and F. Totti, *J. Mater. Chem.*, 2010, **20**, 10747–10754.

3 M. Jaccob, G. Rajaraman and F. Totti, *Theor. Chem. Acc.*, 2012, **131**, 1150.

4 J. E. Matthiesen, D. Jose, C. M. Sorensen and K. J. Klabunde, *J. Am. Chem. Soc.*, 2012, **134**, 9376–9379.

5 G. Rajaraman, A. Caneschi, D. Gatteschi and F. Totti, *Phys. Chem. Chem. Phys.*, 2011, **3**, 3886–95.

6 M. Jaccob, G. Rajaraman and F. Totti, *Theor. Chem. Acc.*, 2012, **131**, 1–11.

7 A. Bencini, G. Rajaraman, F. Totti and M. Tusa, *Superlattices Microstruct.*, 2009, **46**, 4–9.

8 J. Tao, J. P. Perdew, V. N. Staroverov and G. E. Scuseria, *Phys. Rev. Lett.*, 2003, **91**, 146401.

9 S. Grimme, *J. Chem. Phys.*, 2006, **124**, 034108.

10 J. Vandevondele, M. Krack, F. Mohamed, M. Parrinello, T. Chassaing and J. Hutter, *Comput. Phys. Commun.*, 2005, **167**, 103–128.

11 J. Hutter, M. Iannuzzi, F. Schiffmann and J. Vandevondele, *Wiley Interdiscip. Rev. Comput. Mol. Sci.*, 2014, **4**, 15–25.

12 J. VandeVondele and J. Hutter, *J. Chem. Phys.*, 2007, **127**, 114105.

13 G. Bussi, D. Donadio and M. Parrinello, *J. Chem. Phys.*, 2007, **126**, 014101.

14 J. Tersoff and D. R. Hamann, *Phys. Rev. B*, 1985, **31**, 805–813.

15 L. Noodleman, *J. Chem. Phys.*, 1981, **74**, 5737–5743.

16 A. Bencini and F. Totti, *J. Chem. Theory Comput.*, 2009, **5**, 144–154.

17 G. Fernandez Garcia, A. Lunghi, F. Totti and R. Sessoli, 2016, **120**, 16.

18 A. D. Becke, *J. Chem. Phys.*, 1993, **98**, 5648–5652.

19 P. J. Stephens, F. J. Devlin, C. F. Chabalowski and M. J. Frisch, *J. Phys. Chem.*, 1994, **98**, 11623–11627.

20 Y. Zhang and W. Yang, *Phys. Rev. Lett.*, 1998, **80**, 890–890.